J|A|C|S
COMMUNICATIONS

Published on Web 05/03/2003

Exploiting Amyloid Fibril Lamination for Nanotube Self-Assembly

Kun Lu,[†] Jaby Jacob,[§,‡] Pappannan Thiyagarajan,*[,‡] Vincent P. Conticello,*[,†] and David G. Lynn*[,†]

Center for the Analysis of Supramolecular Self-assemblies, Departments of Chemistry and Biology, Emory University, Atlanta, Georgia 30322, Biochemistry and Molecular Biology, University of Chicago, Chicago, Illinois 60637, and Intense Pulsed Neutron Source, Argonne National Laboratory, Argonne, Illinois 60439

Received January 14, 2003; E-mail: dlynn2@emory.edu; vcontic@emory.edu; thiyaga@anl.org

β-Amyloid (Aβ) peptides, a major component of the neuritic plaques associated with Alzheimer's disease (AD), self-assemble into paracrystalline fibrils in solution.[1] Even severely truncated variants of the disease-associated Aβ(1−40) and Aβ(1−42) peptides form fibrils ∼10 nm in diameter. The structural model for Aβ(10−35) suggests that the common fibril diameter could be attained by variation in the degree of lamination. For Aβ(10−35), the lamination of six in-register parallel β-sheets define a 6- × 8-nm fibril (Figure 1).[2] Fibrils formed by the longer Aβ(1−40) may contain 2−4 laminates,[3] while those formed by the shorter Aβ(18−28) peptides contain as many as 24 laminates.[4] Thus, lamination energetics becomes a critical issue in our understanding of fibril structure and stability.

Molecular dynamics simulations of the Aβ(10−35) fibril suggested a dynamic structure in which short stretches of 5−6 residues maintain H-bonding geometry.[5] These H-bonding blocks appear dynamic, moving cooperatively within and between sheets to stabilize the fibril. Therefore, interactions between short peptide segments may limit the overall curvature of the individual sheets and correspondingly increase the degree of lamination in the fibril. On the basis of this hypothesis, very short peptides, notably the critical KLVFFAE region of Aβ[6] previously shown to form fibrils,[7] may display more extensive lamination. This peptide forms antiparallel β-sheets at neutral pH, possibly to satisfy charge complementarity of the N and C termini.[7] To increase the solubility of the peptide and place a single positive charge at the N-terminus to ensure the amphiphilicity that appears critical to parallel β-sheet fibril formation,[2] a 40% acetonitrile/water mixture at pH 2 was selected as solvent for investigation of the self-assembly of this segment.

The seven-residue peptide Aβ(16−22), CH_3CO-KLVFFAE-NH_2, synthesized via standard FMOC solid-phase protocols with both N and C termini capped, was dissolved in an acetonitrile/0.1% TFA aqueous solution adjusted to pH 2. After approximately 20 h, a negative ellipticity at 215 nm, suggestive of β-sheet structure, developed and increased dramatically over the next 10 h (Figure 2). Atomic force microscopy (AFM) revealed the formation of 4-nm-thick, 130-nm-wide sheets at 20 h. With time, these sheets twisted into helical ribbons (Figure 3d). After 30 h, the fibrils were highly homogeneous in diameter, 95 ± 5 nm by AFM (Figure 3a) and 80 ± 5 nm by transmission electron microscopy (TEM) (Figure 3b), with a polydisperse contour fibril length usually >10 μm. The intermediate helical ribbons (Figure 3c,d) twist to give approximately equal numbers of right- and left-handed ribbons in which the edges appear to fuse to form nanotube structures.

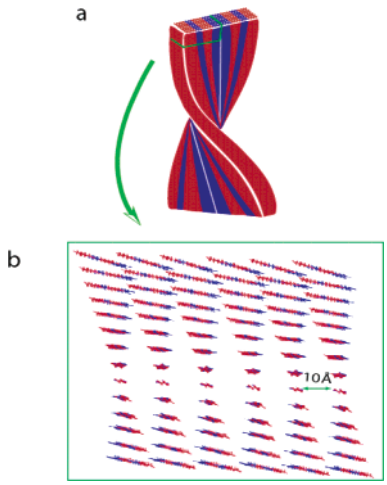

Figure 1. Structural model of the Aβ(10−35) fibril. (a) Paired fibrils of Aβ(10−35), where the individual sheets of each fibril are oriented in parallel to cluster like amino acid domains (red, hydrophilic amino acids; blue, hydrophobic amino acids). The hydrophobic C-terminal amino acids define the interface between the two fibrils. (b) Expanded view of the backbone atoms of the six-sheet laminated Aβ(10−35) fibril orienting like amino acids in parallel and in register along each sheet.[2]

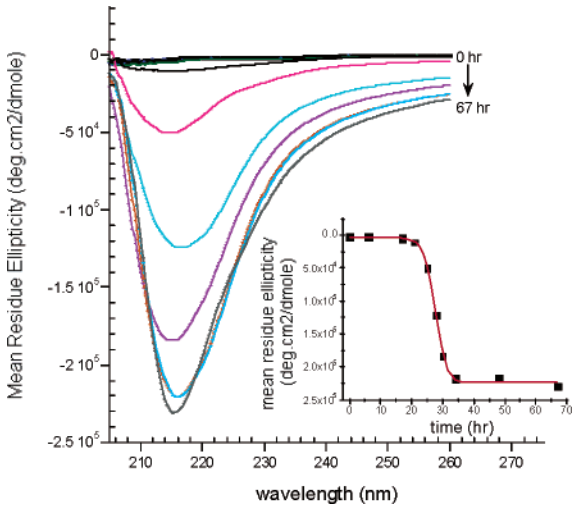

Figure 2. Time-dependent CD spectra of Aβ(16−22). (Inset) Mean residue ellipticity at 215 nm as a function of time for 1.2 mg/mL Aβ(16−22) dissolved in 40% acetonitrile/water with 0.1% TFA (pH 2).

The difference in the diameter observed by AFM and TEM may be due to the varying drying conditions required for the measurements. Small-angle neutron scattering (SANS) and synchrotron small-angle X-ray scattering (SAXS) measurements were used to evaluate the structures in solution. SANS and synchrotron SAXS

[†] Emory University.
[§] University of Chicago.
[‡] Argonne National Laboratory.

10.1021/ja0341642 CCC: $25.00

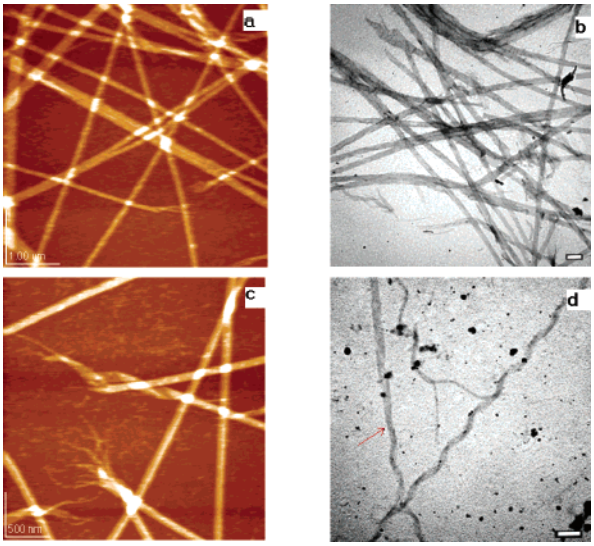

Figure 3. AFM (a, c) and TEM (b, d) micrographs of fibrils formed by Aβ(16−22). Peptides were allowed to assemble for two weeks (a, b), 23 h (c), or 30 h (d). Red arrow shows the transition from the helical ribbon to the fused nanotube. Scale bar in TEM, 200 nm.

measurements were carried out at SAND at IPNS and BESSRC-CAT at APS, respectively. Small-angle scattering intensity, $I(Q)$, can be described by

$$I(Q) = I_0 n(\Delta\rho)^2 V^2 P(Q) + I_b \qquad (1)$$

for a dilute system of scattering particles, where I_0 is an instrument constant, n is the number density of particles, $\Delta\rho$ is the difference in scattering length density (contrast) between particles and solvent, V is the volume of particles, I_b is the flat background intensity, and $P(Q)$ is the particle form factor. Q is the momentum transfer, given by $Q = (4\pi/\lambda)\sin(\theta/2)$, where λ is the neutron or X-ray wavelength and θ is the scattering angle. Several models were investigated, but only $P(Q)$ for hollow cylindrical particles accurately fit the data:

$$P(Q) = \int_0^1 \left(\frac{1}{1-(R_2/R_1)^2}\right)^2 \left[\frac{2J_1(QR_1(1-x^2)^{0.5})}{QR_1(1-x^2)^{0.5}} - \frac{(R_2/R_1)^2 2J_1(QR_2(1-x^2)^{0.5})}{QR_2(1-x^2)^{0.5}}\right]^2 \left(\frac{\sin(QHx/2)}{QHx/2}\right)^2 dx \qquad (2)$$

Here, R_1 is the outer radius and R_2 the inner radius; H is the height of the cylinder, and $J_1(x)$ is the Bessel function of the first order. Oscillations in $I(Q)$ characteristic of the form factor for hollow cylindrical particles (eq 1) were observed in both SANS and SAXS data (Figure 4). The difference in $I(Q)$ between SAXS and SANS data is due to the different contrast ($\Delta\rho$) in the two cases—electron scattering length difference in SAXS and neutron scattering length difference in SANS. This produces only a vertical shift between the two data sets. Although SANS and SAXS data exhibit peaks at the same Q values, the number of oscillations and the depth of the valleys are larger in the SAXS data due to the high brilliance of the synchrotron source and the higher resolution of the detector used. We fitted the SAXS and SANS data using eqs 1 and 2 to obtain the cross-sectional dimensions of the nanotube. From Figure 4, it is clear that the data are well described by a monodisperse system of hollow cylinders with an outer radius of 26 nm and a wall thickness of 4 nm. The length is too large to be determined

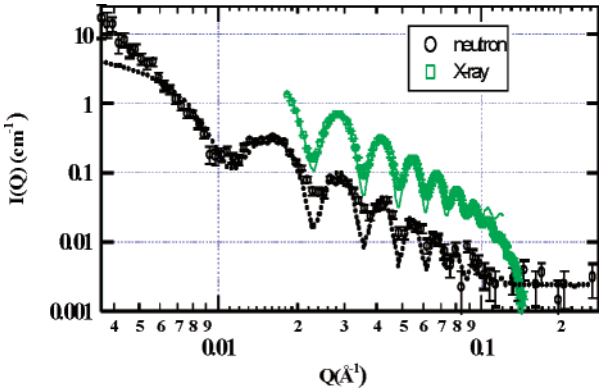

Figure 4. Measured SANS (black) and SAXS (green) data for 1.2 mg/mL Aβ(16−22) at pH 2 in 40% acetonitrile-d_3/D_2O after 6 days of incubation, along with the fit to the data using the form factor for a hollow cylinder. Open points with error bars are data, and the lines/points are the theoretical scattering curves of a hollow cylinder. The dimensions of the tubular fibril are identical by both SANS and SAXS measurements.

by the small-angle scattering measurements, and the polydispersity in the length may explain the discrepancy between the SANS data and the modeled curve at the low Q ($Q < 0.006$ Å^{-1}) region. The measured fibril diameter (52 nm) in solution from SAXS is different from those from AFM and TEM images. However, a 52-nm-o.d. tubular fibril, collapsed on the silicon surface, will give a width of πr, 82 nm in this case and in agreement with the TEM measurements. The 10−15-nm tip width further compromises the precision in the AFM measurements in the surface plane.

The 4-nm thickness of the tube is roughly twice the length of the Aβ(16−22) peptide. This doubling of the peptide length, also present in the Aβ(10−35) duplex fibril (Figure 1a), suggests that the tubular wall is composed of a peptide bilayer. Indeed, Zhang et al. recently observed branched nanotubes formed from surfactant-like peptides containing a hydrophilic headgroup of charged aspartic acids and a lipophilic tail made of leucine, alanine, or valine.[8] These structures were modeled as a bilayer assembly on the basis of TEM measurements.

The nanotube assemblies of Aβ(16−22) form in H_2O at pH 2, and the rates are much faster than in 40% acetonitrile. Increasing the KCl concentration from 0 to 20 mM in 40% acetonitrile accelerates the rate of both the nucleation and propagation steps. For example, the observed lag time is reduced from 21 h in 0 mM KCl to <5 h in 20 mM KCl, indicating a significant dielectric dependence of Aβ(16−22) nanotube nucleation. The preformed nanotubes also melt upon heating to 80 °C and reassemble on cooling. Such dependence on media dielectric and temperature is common to lipid bilayer assembly.

The proposed bilayer model (Figure 5) places the charged N-terminal lysine residues at the solvent-exposed surface, while the hydrophobic residues are sequestered internally. The backbone H-bonds are on the long axis of each leaflet, fixing a peptide backbone spacing at 5 Å between adjacent parallel, in-register β-strands. The sheet width, defined by the lamination dimension, is assumed to maintain the 10-Å spacing between the individual parallel β-sheets. Correcting for the overestimate by AFM, the initial bilayer sheet is around 130 nm wide, and therefore composed of 130 laminates. Therefore, the simple bilayer proposed for the Aβ(10−35) duplex fibril with only six laminates (Figure 1a) has been dramatically extended merely by shortening the peptide length to seven residues. For the ribbon to twist so that the ends meet and yet maintain the same number of laminates, the outer leaflet requires a periodicity of 214 nm, while that for the inner leaflet would be

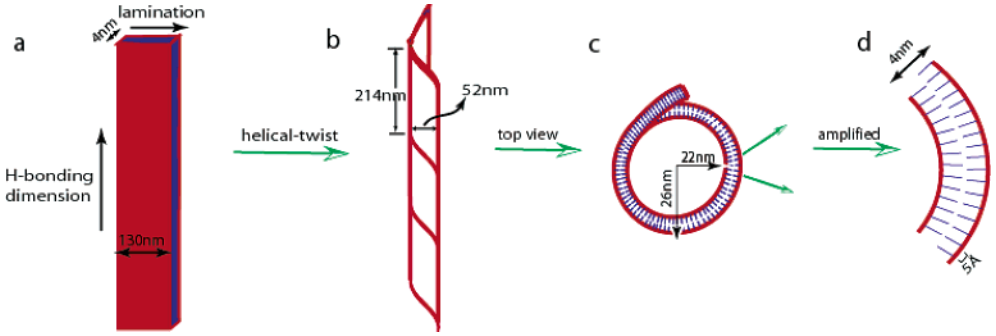

Figure 5. Model for self-assembly of the peptide nanotubes. (a) A flat rectangular bilayer, 130 nm wide × 4 nm thick, with each leaflet composed of β-sheets, and the corresponding backbone H-bonds, oriented on the long axis, and β-sheet lamination defining the 130-nm bilayer width. (b) The coiled tubular fibril with an outer diameter of 52 nm and an outer helical pitch of 214 nm. (c) Top view of the 44-nm internal cavity. (d) Amplified view of the wall with a thickness of 4 nm and the distance between each parallel β-strand being the backbone H-bond distance of 5 Å.

383 nm.[9] This pitch requires a 0.42° and 0.23° offset between adjacent outer and inner Aβ(16−22) strands, respectively. In contrast, the offset required for each Aβ(10−35) strand in the fibril (Figure 1b) is 1.6°. These results are therefore consistent with the hypothesis that shorter peptides can energetically access a more planar β-sheet and are able to maintain more extensive lamination order than seen in longer amyloid peptides.

The peptide nanotubes therefore merely extend the Aβ(10−35) fibril dimer model (Figure 1) in lamination order. The resulting structures are similar to those formed by several other amphiphiles, including lipids,[10] bile acids,[9] phenyl glucosides,[11] diacetylenic aldonamides,[12] and double-chain glutamate derivatives,[13] suggesting that some intrinsic characteristics in the self-assembly process are common to various molecular frameworks. While more work will be required to refine the structural and energetic details of self-assembly, it is clear that the inherent stability, so characteristic of amyloid fibril assemblies, can now be extended to various structures,[14] including soluble nanotube construction. Such robust and persistent self-assembling nanotubes with positively charged surfaces of very different inner and outer curvature now offer a unique, robust, and easily accessible scaffold for nanotechnology.

Acknowledgment. We thank DOE ER15377 (V.P.C. and D.G.L.), Emory University, the Integrated Microscopy and Micro-analytical Facility, NSF (CHE-0131013) for the JASCO CD, C.L. Emerson for AFM instrumentation, and the Packard Foundation Interdisciplinary Science Program (99-8327) to D.G.L. and P.T. for financial support. This work benefited from use of IPNS and BESSRC-CAT at APS, funded by the U.S. DOE, BES under contract W-31-109-ENG-38 to the University of Chicago.

Supporting Information Available: Additional models for the SAXS data (PDF). This material is available free of charge via the Internet at http://pubs.acs.org.

References

(1) (a) Lynn, D. G.; Meredith, S. C. *J. Struct. Biol*. **2000**, *130*, 153−173. (b) Morgan, D. M.; Dong, J.; Jacob, J.; Lu, K.; Apkarian, R. P.; Thiyagarajan, P.; Lynn, D. G. *J. Am. Chem. Soc*. **2002**, *124*, 12644−12645. (c) Serpell, L. C. *Biochim. Biophys. Acta* **2000**, *1502*, 16−30. (d) Costa, P. R.; Kocisko, D. A.; Sun, B. Q.; Lansbury, P. T., Jr.; Griffin, R. G. *J. Am. Chem. Soc*. **1997**, *119*, 10487−10493. (e) Teplow, D. B. *Amyloid: Int. J. Exp. Clin. Invest.* **1998**, *5*, 121−142. (f) Lansbury, P. T., Jr.; Costa, P. R.; Griffiths, J. M.; Simon, E. J.; Auger, M.; Halverson, K. J.; Kocisko, D. A.; Hendsch, Z. S.; Ashburn, T. T.; Spencer, R. G. S.; Tidor, B.; Griffin, R. G. *Nature Struct. Biol*. **1995**, *2*, 990−998.

(2) Burkoth, T. S.; Benzinger, T. L. S.; Urban, V.; Morgan, D. M.; Gregory, D. M.; Thiyagarajan, P.; Botto, R. E.; Meredith, S. C.; Lynn, D. G. *J. Am. Chem. Soc*. **2000**, *122*, 7883−7889.

(3) Garzon-Rodriguez, W.; Sepulveda-Becerra, M.; Milton, S.; Glabe, C. G. *J. Biol. Chem.* **1997**, *272*, 21037−21044.

(4) Kirschner, D. A.; Inouye, H.; Duffy, L. K.; Sinclair, A.; Lind, M.; Selkoe, D. J. *Proc. Natl. Acad. Sci. U.S.A.* **1987**, *84*, 6953−6957.

(5) (a) Morgan, D.; Lynn, D. G.; Lakdawala, A. S.; Snyder, J. P.; Liotta, D. C. *J. Chin. Chem. Soc*. **2002**, *49*, 459−466. (b) Lakdawala, A. S.; Morgan, D. M.; Liotta, D. C.; Lynn, D. G.; Snyder, J. P. *J. Am. Chem. Soc*. **2002**, *124*, 15150−15151.

(6) (a) Wood, S. J.; Wetzel, R.; Martin, J. D.; Hurle, M. R. *Biochemistry* **1995**, *34*, 724−730. (b) Fay, D. S.; Fluet, A.; Johnson, C. J.; Link, C. D. *J. Neurochem.* **1998**, *71*, 1616−1625. (c) Tjernberg, L. O.; Näslund, J.; Lindqvist, F.; Johansson, J.; Karlström, A. R.; Thyberg, J.; Terenius, L.; Nordstedt, C. *J. Biol. Chem.* **1996**, *271*, 8545−8548.

(7) Balbach, J. J.; Ishii, Y.; Antzutkin, O. N.; Leapman, R. D.; Rizzo, N. W.; Dyda, F.; Reed, J.; Tycko, R. *Biochemistry* **2000**, *39*, 13748−13759.

(8) Vauthey, S.; Santoso, S.; Gong, H.; Watson, N.; Zhang, S. *Proc. Natl. Acad. Sci. U.S.A.* **2002**, *99*, 5355−5360.

(9) Chung, D. S.; Benedek, G. B.; Konikoff, F. M.; Donovan, J. M. *Proc. Natl. Acad. Sci. U.S.A.* **1993**, *90*, 11341−11345.

(10) (a) Schnur, J. M. *Science* **1993**, *262*, 1669−1676. (b) Fuhrhop, J.; Helfric, W. *Chem. Rev.* **1993**, *93*, 1565−1582.

(11) Jung, J. H.; John, G.; Yoshida, K.; Shimizu, T. *J. Am. Chem. Soc*. **2002**, *124*, 10674−10675.

(12) Frankel, D. A.; O'Brien, D. F. *J. Am. Chem. Soc*. **1991**, *113*, 7436−7437.

(13) Nakashima, N.; Asakuma, S.; Kunitake, T. *J. Am. Chem. Soc.* **1985**, *107*, 509−510.

(14) (a) Lashuel, H. A.; LaBrenz, S. R.; Woo, L.; Serpell, L. C.; Kelly, J. W. *J. Am. Chem. Soc*. **2000**, *122*, 5262−5277. (b) Kirschner, D. A.; Elliott-Bryant, R.; Szumowski, K. E.; Gonnerman, W. A.; Kindy, M. S.; Sipe, J. D.; Cathcard, E. S. *J. Struct. Biol*. **1998**, *124*, 88−98.

JA0341642